Synergistic Effect Enables Aqueous Zinc-Ion Batteries to Operate at High Temperatures

Changlei Zhuang, Siwen Zhang,* Zhi Gen Yu, Jinzhang Yang, Ying Sun, Hanyu Wen, Haokun Wen, Hui Li, Bosi Yin,* and Tianyi Ma*

The performance of aqueous zinc-ion batteries (AZIBs) at high temperatures (HT) is severely compromised by active water corrosion, parasitic reactions, and dendrite growth. Herein, zinc trifluoroacetate is introduced at a low concentration (0.2 m), dissolved in triethyl phosphate (TEP) and H_2O. The active water is suppressed due to the reconstructed original hydrogen bond network, which helps inhibit parasitic reactions and severe corrosion. Meanwhile, a solid electrolyte interphase (SEI) formed on the zinc anode due to the decomposition of the introduced zinc salt. The high-tolerance SEI physically separates the electrolyte and anode, reducing the corrosion caused by active water. Moreover, TEP, as a prevalent fire-retardant cosolvent, can preferentially anchor on the zinc and the $NH_4V_4O_{10}$ (NVO) full cells achieve 1400 cycles at 60 °C. This work offers a promising solution to prompt the commercialization of AZIBs at HT.

1. Introduction

Lithium-ion batteries (LIBs) have gained great popularity in recent years, nevertheless, it is subjected to scarcity and flammable organic electrolytes.[1] Thus, other kinds of metal batteries have been proposed, among which aqueous zinc- ion batteries (AZIBs) are one of the most promising alternatives,[2] profiting from its intrinsic advantages of safe, inexpensive, low redox potential (−0.762 V vs SHE), high theoretical capacity (820 mAh g^{-1}, 5854 mAh cm^{-3}), and ample resource.[3] Many efforts have been made to direct ZIBs in aggressive conditions, especially in low temperatures (LT). Yet an increasingly expanded application scenario, such as special operations, requires more findings to exhibit satisfactory performance at high temperatures (HT).[1] Nevertheless, the advancement of HT AZIBs is still sluggish due to the following dilemmas. From a cathode perspective, extreme condition exacerbates host structural collapses resulting from active water in electrolyte which serves as the ions-transfer arena, contributing to capacity decay, and triggering cell failure further.[4] On electrolyte/electrode interfacial sides, the Zn anode inevitably confronts parasitic reaction and dendrite growth because of the zinc ion desolvation process at rising temperatures.[5] In addition, the ceaseless evaporation of water content causes the electrolyte to dehydrate and zinc salt to crystallize.[1] All of these greatly un- dermine satisfied Coulombic efficiency (CE) and cycle stability, and worse is that it deteriorates when at HT.[6] For example,

C. Zhuang, S. Zhang, J. Yang, Y. Sun, H. Wen, H. Wen, B. Yin
Institute of Clean Energy Chemistry
Key Laboratory for Green Synthesis and Preparative Chemistry of Advanced Material
College of Chemistry
Liaoning University
Shenyang 110036, P. R. China
E-mail: zhangsiwen@lnu.edu.cn; yinbosi@lnu.edu.cn
Z. G. Yu
Agency for Science
Technology and Research (A*STAR)
Institute of High Performance Computing (IHPC)
1 Fusionopolis Way, #16-16 Connexis, Singapore 138632, Republic of Singapore
H. Li, T. Ma
Centre for Atomaterials and Nanomanufacturing (CAN)
School of Science
RMIT University
Melbourne, VIC 3000, Australia
E-mail: tianyi.ma@rmit.edu.au
H. Li, T. Ma
ARC Industrial Transformation Research Hub for Intelligent Energy Efficiency in Future Protected Cropping (E2Crop)
Melbourne, VIC 3000, Australia

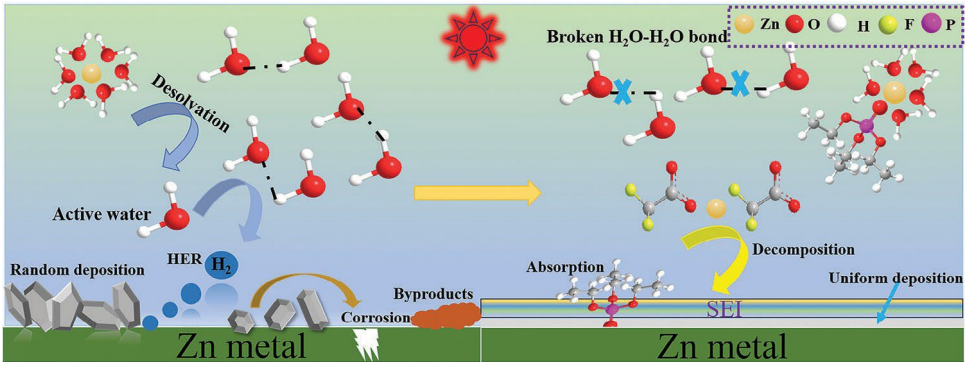

Figure 1. Schematic illustration of hydrogen bond network, solvation structure, and SEI formation in different electrolytes.

Wang et al. reported diethylene glycol monoethyl ether (DG) to impair the initial hydrogen bonding network and restructure the solvation structure in 2 m $Zn(OTF)_2$ as an electrolyte additive, which enabled AZIBs operating at HT up to 65 °C.[7] Similarly, Yun et al. regulated the dipolar–dipolar and ion–dipolar interactions by introducing tetramethylurea (TMU) into 2 m $Zn(OTf)_2$ to weaken the hydrogen-bond network and lower water content in the Zn^{2+} solvation shell, which brought AZIBs into 90 °C operation.[8] These dedicated efforts fulfilled the drawbacks of AZIBs at HT operation to some extent, nevertheless, expensive salt and its high concentration characterized by easy crystallization compromised the natural advantage of AZIBs, hindering large-scale application.[9] Inspired by this, exploring novel zinc salts together with low concentration is considered a promising alternative to tackle these issues.

Herein, zinc trifluoroacetate in its cosolvent was proposed, featuring low cost, outstanding thermal stability, high design flexibility, and easy preparation.[10] By employing the above electrolyte, the hydrogen bond network existing in the original electrolyte is reconstructed, restraining the occurrence of a notorious hydrogen evolution reaction (HER). Additionally, introduced zinc salt also tends to decompose to form a solid electrolyte interphase (SEI) upon Zn anode, acting as a physical barrier to prevent HT-triggered active water,[11] which effectively inhibits dendrites and active water corrosion. Meanwhile, triethyl phosphate (TEP), as a stable cosolvent with a high boiling point could absorb on the zinc sheet, forming a protective layer against HT. It also alters the electric double layer (EDL) structure to repel more H_2O from the inner Helmholtz plane (IHP),[12] prompting the formation of SEI, which greatly protects the Zn anode from active water corrosion. Taking advantage of the synergistic effect of this electrolyte (**Figure 1**), a satisfied HT performance is achieved. As a result, under 60 °C, the Zn||Zn symmetrical cells survived up to almost 2000 h with the current density of 0.1 mA cm^{-2}, and coupling with the Zn||$NH_4V_4O_{10}$ (NVO) sustained almost 1400 cycles under 1 A g^{-1}, with a capacity retention rate of 63.23%. This work offers high participation to advance a series of metal batteries standing by AZIBs to HT application.

2. Results and Discussion

A wide array of spectral characterization was carried out to investigate the influence of TEP of various concentrations on zinc solvation structure and its role in hydrogen bond network reconstruction. As **Figure 2a** demonstrates, the H peak in the nuclear magnetic resonance (NMR) of D_2O is located at 4.695 ppm, when ZFC with 0 TEP was involved, a notable shift to a lower field was witnessed due to a vigorous interaction between Zn^{2+} and H_2O due to decreased electron density around water molecules and the weakening of proton shielding effect.[5] With the increasing proportion of TEP, the H peak gradually went back to a higher field, corresponding to the robust interaction between the Zn^{2+} ion and H_2O was undermined, and H_2O molecules were unleashed from the original Zn^{2+} solvation shell. Simultaneously, the H peak belonging to TEP could be witnessed a moving forward to a lower field, suggesting a robust interaction between TEP and H_2O, during which the original hydrogen bond network was impaired.[13] Furthermore, Raman spectrum in Figure 2b and Fourier transform infrared spectroscopy (FTIR) observes a palpable shift no matter stretching vibration of O—H within the range of 3000–3700 cm^{-1} or bending vibration of O—H within the range of 1550–1750 cm^{-1} when TEP concentration increased in ZFC electrolytes (Figure 2c), indicating that TEP could break the hydrogen bond network between tetrahedral water molecules and alter the coordination structure of water.[14] Simultaneously was that the FTIR peaks of P = O stretching vibration located at 1252 cm^{-1} and the -PO_3 groups located at 1179 cm^{-1} from TEP molecules shifted to the high wavenumbers, indicating that an extensive interaction between TEP and Zn^{2+} for higher Gutmann donors in TEP (26 kcal mol^{-1}) against H_2O (18 kcal mol^{-1}) and taking places of H_2O from solvation sheath.[15] Ionic conductivity is a significant indicator to evaluate the performance of electrolytes. To explore the relationship between solvent components, as Figure S1 (Supporting Information) suggests the resistance of prepared electrolytes surges along with TEP increasing gradient concentration, corresponding to an attenuated ionic conductivity value for increased viscosity from TEP solvent. To simplify the experiment, a series of electrochemical performances were evaluated to get the optimal combination (Figure S2, Supporting Information), and a counterpart was selected as well (Figure S3, Supporting Information). Figure S2 (Supporting Information) witnessed that with an increase in TEP content, the lifetime of Zn//Zn symmetric cell and Zn//Cu half cell were extended except for 100 TEP group. A delicate trade-off was established between electrochemical performance and ionic conductivity and the former was attached to more significant. To make

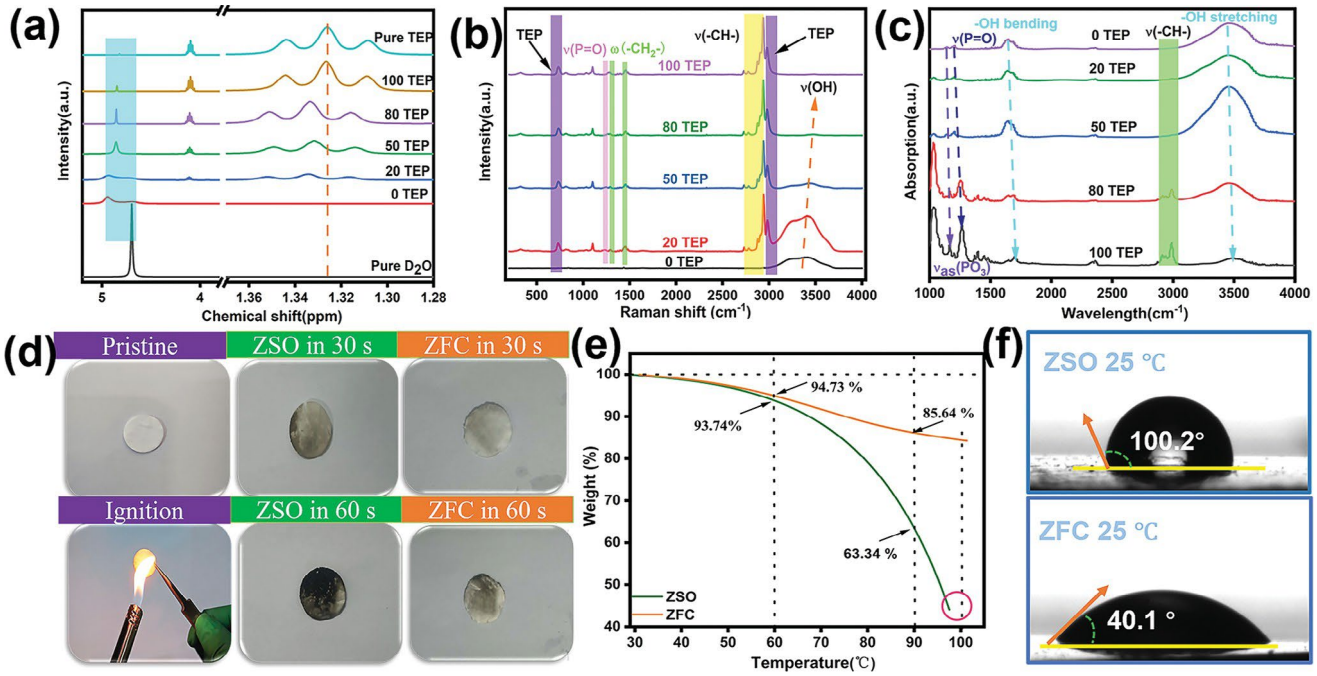

Figure 2. a) ^{1}HNMR spectra of D_2O, pure TEP, and ZFC with different concentrations of TEP. b) Raman spectra of with different concentrations of TEP. c) FTIR spectra with the above electrolytes. d) Ignition test of ZSO and ZFC electrolyte. e) TG curves of different electrolytes in a nitrogen atmosphere from 30 to 100 °C. f) Contact angle measurement of ZFC and ZSO electrolyte.

a comparison of the above electrolytes, a wide range of experiments comparing the flammability and thermal stability of the electrolyte were measured in aggressive conditions. Ignition test demonstrated that the ZFC electrolyte featured non-flammable prosperity to maintain the separator white and moist in the fire for 30 and 60 s, respectively, whereas the blackened separator of ZSO for high evaporation of contained electrolyte for continuous burning within 1 min (Figure 2d). Likewise, the thermogravimetry (TG) technique was conducted to determine the above electrolyte thermostability.

ZFC electrolyte possessed highly enhanced thermal stability with weight retention of 85.64% against 63.34% of ZSO when the temperature reached 90 °C and remained at 84.4% when reached 100 °C, but ZSO failed to reach 100 °C due to continued evaporation (Figure 2e). Both electrolyte weights were recorded every 30 min under 60 °C to simulate electrolyte evaporation in an open environment if the cell swelled and cracked because of severe HER (Figure S4, Supporting Information). The ZFC electrolyte exhibited low volatility with 98.58% remaining of the original weight after exposing to the atmosphere for 300 min (Figure S5, Supporting Information), whereas the reference aqueous electrolyte decreased to 98% (Figure S6, Supporting Information), which suggested a thermostability electrolyte established for dominant organic component and reconstructed hydrogen bond network. Additionally, a sessile drop contact angle was used to compare the zincophilic of the above electrolytes, affecting Zn nucleation behaviors further. ZSO presented a high contact angle of 100.2° on zinc metal, but decreased dramatically to 40.1° of ZFC electrolyte (Figure 2f), demonstrating that ZFC had high wettability deriving from strong preferential absorption of TEP upon the zinc metal, thus laying a great foundation for excellent zinc plating/stripping efficiency on the electrode/electrolyte interface.[14] To certify in a quantifiable manner that a vigorous preferentially absorption of TEP upon the Zn panel, the electric double layer capacitance (EDLC) under different scan rates was measured at 60 °C (Figure S7, Supporting Information). Compared with 32.04 μF cm^{-2} of ZSO, the value reduced to 27.09 μF cm^{-2} in ZFC electrolyte, attributed to the adsorption of TEP upon the surface of the Zn electrode, thus shrinking the effective electrochemical surface area,[16] which could benefit the construction of SEI formation in zinc-ion plating/striping process.

To visualize the zinc-ion plating/striping efficiency in terms of macro and micro perspectives, detached zinc sheet cycling at HT from the deposition side was photographed with fresh zinc sheet as substrate featuring an intrinsic uniform property (Figure S8, Supporting Information). As Figure S9 (Supporting Information) shows, the zinc sheet in ZSO electrolyte exhibited disorganized clusters compared with ZFC in flat sedimentation morphology, agreeing well with the above argument. The scanning electron microscopic (SEM) under various cycles provided more visual evidence about the homogeneous sedimentation and densely, smoothly packed morphology with zinc deposited parallel to the substrate at 60 °C under the condition of 1 mA cm^{-2} and 0.25 mAh cm^{-2}, as cells proceeded to different cycles (**Figures** 3a and S10a, Supporting Information). Conversely, Zn deposition randomly and porously with unregulated clustered dendrites, and sunken pits on account of active water corrosion fueled by HT, as shown in Figure 3b and Figure S10b (Supporting Information), all results matched well with optical images as illustrated in Figure S9 (Supporting Information). High-resolution transmission electron microscopy (HRTEM) characterization offered nano-level perspectives visually into the SEI microstructure

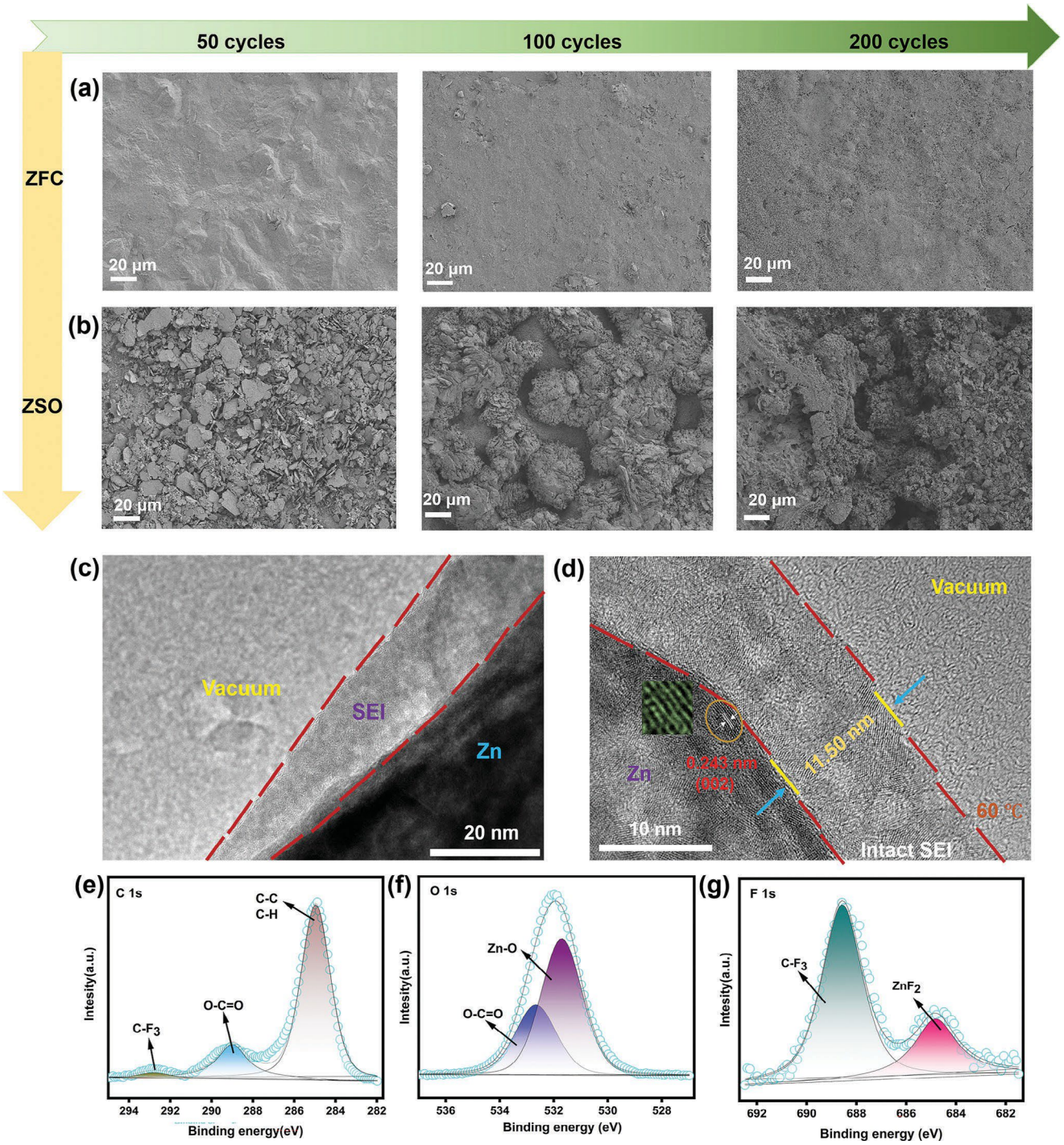

Figure 3. a) SEM images of zinc sheet in ZFC electrolyte after 1 mA cm^{-2} and 0.25 mAh cm^{-2} for 50th, 100th, and 200th cycles at 60 °C, respectively. b) SEM images of zinc sheet in ZSO electrolyte after 1 mA cm^{-2} and 0.25 mAh cm^{-2} for 50th, 100th, 200th cycles at 60 °C, respectively. c,d) TEM images of cycled zinc sheet in ZFC electrolyte under different magnificent. e) XPS C 1s and f) O 1s spectra and g) F 1s spectra of zinc sheet in ZFC electrolyte after 1 mA cm^{-2} and 0.25 mAh cm^{-2} for 50 cycles.

establishment on Zn anode in ZFC electrolyte, which is visible clearly to intact structure in conformal SEI layer with ≈11.50 nm thickness as Figure 3c,d and Figure S11a (Supporting Information) shown, which is believed to provide a protective shield physically against active water corrosion powered by HT.[17] Notably, fast Fourier transform (FFT) analysis calculated the crystal plane spacing of the Zn crystals (2.43 Å) (Figure 3d), agreeing well with the Zn (002) crystal plane acquired from its XRD database, resulting from a preferential absorption behavior of TEP on Zn plane as Figure S7 (Supporting Information) discussed

before. Nevertheless, a stark comparison was erected comparing to Figure S11b (Supporting Information), imperceptible and thinner SEI in ZSO electrolyte, which was vulnerable to receiving active water corrosion and inhibiting pronounced dendrites growth.

Meanwhile, to precisely determine the composition of SEI formed on the Zn surface, X-ray photoelectron spectroscopy (XPS) was further carried out. Specific elements were detected from cycled zinc sheets under the conditions of 1 mA cm^{-2} and 0.25 mAh cm^{-2} for 50 cycles in different electrolytes (Figure S12, Supporting Information). The cycled Zn anode displayed conspicuous C 1s and O 1s spectra belonging to C-F_3, O—C═O, C—H/C—C, Zn—O groups, respectively (shown in Figure 3e,f), and as illustrated in Figure 3g, the characteristic peaks of the C–F_3 species (≈688.58 eV) and inorganic ZnF_2 signs (≈684. 78 eV), as well as a trace amount of $Zn_3(PO_4)_2$ (≈134.78 eV) was evidenced clearly on the surface of the Zn anode after cycling in the ZFC electrolyte (Figure S13, Supporting Information), these species formed suitable thickness SEI, which is believed to inhabit vertical dendrites growth from high surface energy sites and alleviate active water attack.[17] Nevertheless, no similar peak was identified in C 1s spectra as Figure S14a (Supporting Information), and SO_4^{2-}, SO_3^{2-}, ZnS, and ZnO inorganic phases featuring thinly and unevenly were identified as Figure S14b,c (Supporting Information) exhibited. According to the experimental results of XPS, the main component of SEI was the decomposition product of zinc trifluoroacetate and the involvement of TEP. Inorganic phases such as the ZnF_2-rich layer and $Zn_3(PO_4)_2$-rich layer featuring high toughness could effectively inhibit notorious zinc dendrites, thereby promoting the uniform deposition of zinc ions,[14,18] as vividly witnessed in Figure 3a of the SEM images. The organic phase, such as $-COO^-$ rich layer with high viscoelasticity generated by the decomposition of trifluoroacetate anion could accommodate a large volume change, which was especially pronounced at HT in the Zn stripping/plating process. Interestingly is that the formed SEI layer does not hinder the charge transport kinetics, but restricts the potential side reactions such as HER and Zn metal corrosions, and prompts the uniform Zn deposition as well[14,19] (Figure S14d, Supporting Information).

To investigate the zinc ion behavior at HT, the chronoamperometry (CA) technique was employed to track Zn^{2+} diffusion and nucleation behavior along the zinc sheet under a fixed voltage of −150 mV as **Figure 4**a unveiled. In ZSO electrolyte, an undesired 2D diffusion contained 85 s, with mounting response current, referring to plumules period of cliff dendrites for "tip effect",[20] and then processing into 3D diffusion. By stark contrast, ZFC electrolytes experienced a placid 3D diffusion process, hence uncontrolled dendrites were effectively inhibited.[21] Moreover, charge transfer impedance (Rct) under various temperatures was measured, thus desolvation energy (Ea) was calculated further based on the Arrhenius equation. A comparison of 27.13 kJ mol^{-1} of ZFC electrolyte and 34.27 kJ mol^{-1} of ZSO electrolyte (Figure S15, Supporting Information), suggested that a less Zn^{2+} desolvation barrier due to altered solvation shell and formed SEI layer, fueling reaction kinetics to gain a better electrochemical performance.[22] And nucleation overpotential (NOP) was measured at HT as well (Figure 4b), ZFC elevated NOP to 189.8 mV compared with 100 mV of ZSO, owing to TEP preferentially anchored on the Zn plane, not only modulating EDL structure and casting out water from IHP, but also tuning zinc flux to achieve fine deposition.[15,23] Cyclic voltammetry (CV) profiles ranging from −0.4 to −0.9 V of Zn||Cu half cells assembling with ZFC and ZSO electrolytes were presented in Figure S16 (Supporting Information). A single peak in the plot suggested that the zinc-ion plating/stripping process could not be disrupted by HT operation.[24] And evaluated NOP value of 25.5 mV agreed well with Figure 4b. Anticorrosion performance was further carried out at HT utilizing Tafel and linear scanning voltammetry (LSV) techniques.[16]

As Figure 4c and Figure S17 (Supporting Information) exhibit, ZFC displays alleviated self-corrosion issues and parasitic reactions than ZSO, helping to effectively restrain byproducts and HER triggered by HT.[25] Fresh zinc sheets were soaked in the above electrolyte for one week to demonstrate anticorrosion performance at HT intuitively. A flat and smooth surface appeared in the ZFC electrolyte whilst rough and irregular flakes were staked on the Zn electrode in the ZSO electrolyte from centimeter (Figure S18a, Supporting Information) and micron level (Figure S18b–e, Supporting Information). Comparing with Figures S19,S20 (Supporting Information), one can conclude that SEI was formed to inhibit parasitic reactions stemming from ZFC decomposition during idle time at HT. Meanwhile, it is self-evident that byproducts emerged in ZSO for thinner and deformed SEI as certified in Figure S11b (Supporting Information). A wide range of electrochemical experiments was conducted to evaluate the Zn plating/stripping performance. The rate performance for Zn||Zn symmetrical cells was tested, and ZFC displayed satisfied performance with ≈100% CE (Figure 4d), nevertheless, ZSO was in short circuit and failure finally when beyond 150 h. Zinc-ion plating/stripping process was evaluated by Zn||Cu half cells on various conditions under 60 °C (Figure 4e and Figure S21, Supporting Information). Under the condition of 2 mA cm^{-2} and 0.25 mAh cm^{-2}, ZFC survived 650 cycles with an average CE of 97.87%, whilst a cell failed beyond 105 cycles in ZSO for pristine reaction,[26] the same phenomenon was witnessed under the condition of 2 mA cm^{-2} and 0.5 mAh cm^{-2} as Figure S22 (Supporting Information) detailly reviled, affirming the excellent CE performance of ZFC under harsh conditions. A series of galvanostatic charge-discharge (GCD) tests determined the reversibility of Zn plating/stripping efficiency. When the current density was set to 0.1 mA cm^{-2} with the capacity of 0.1 mAh cm^{-2} (Figure 4f), ZFC was capable of circulating 2000 h stably and ZFC suffered failure when beyond 500 h comparatively for serious dendrites growth. When the current density increased to 0.5 mA cm^{-2} with the capacity of 0.25 mAh cm^{-2} (Figure 4g), ZFC could still survive 700 h, while ZSO failed within 100 h and cell inflation happened during the GCD process because of severe HER. Other test conditions are served in Figure 4h and Figure S23 (Supporting Information) reiterated ZFC is advantageous against ZSO. By the way, the Aurbach method was utilized subsequently to assess the reversibility of the zinc metal anode with the above electrolytes under 60 °C by Zn|| Cu half cells[27] (Figure S24, Supporting Information). ZFC electrolyte exhibited CE of 97.72%, higher than that of the ZSO (94.48%), suggesting a superior performance of ZFC at HT operation. To conclude, Figure 4i demonstrates the lifespan under various current densities and capacity of ZFC displaying excellent performance than ZSO. In addition, a comparison of our tested performance with other published literature as Figure S25 and Table S1

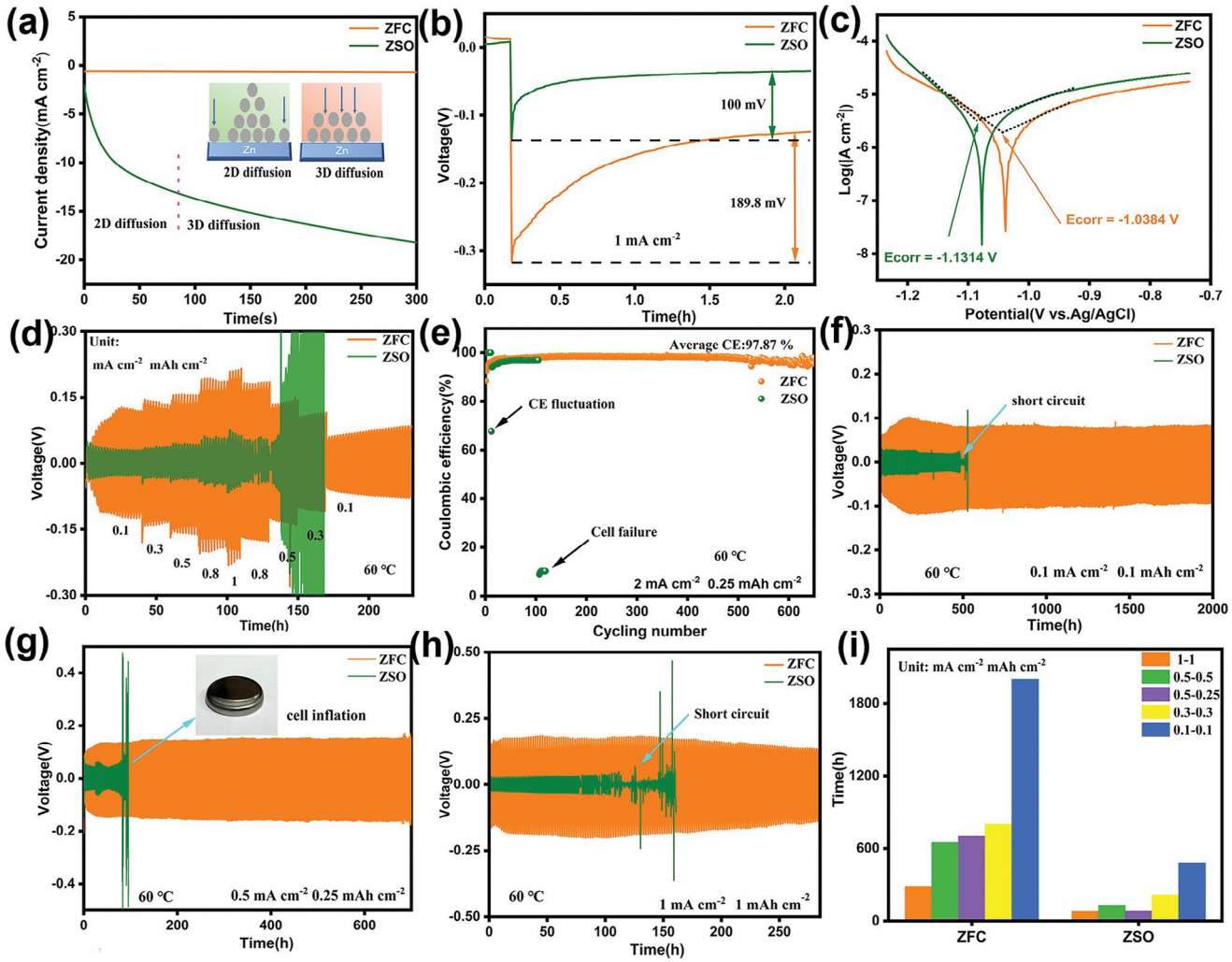

Figure 4. a) CA curves of ZFC and ZSO under a fixed potential of −150 mV at 60 °C. b) The measured NOP value for Zn deposition at 60 °C. c) Tafel plot tested at 60 °C. d) The rate performance of the above electrolyte at 60 °C. e) Long-term performance of Zn plating/stripping efficiency on Zn||Cu half cells under the condition of 2 mA cm^{-2} and 0.25 mAh cm^{-2}. Lifespan performance of Zn||Zn symmetrical cells under the condition of f) 0.1 mA cm^{-2} and 0.1 mAh cm^{-2} and g) 0.5 mA cm^{-2} and 0.25 mAh cm^{-2}, inset: optical image of Zn||Zn symmetrical cell with ZSO electrolyte after cycled, and h) 1 mA cm^{-2} and 1 mAh cm^{-2}. i) Survive time comparison of Zn||Zn symmetrical cells with above electrolyte at 60 °C.

(Supporting Information) unveiled that ZFC electrolyte has outstanding potential for HT application.

To further verify its practical performance and temperature adaptability at 60 °C, various performances of Zn||NVO batteries were assembled coupling with ZFC and ZSO electrolytes. First, the NVO nanosheet was prepared and successfully verified by XRD (Figure S26, Supporting Information), SEM, and corresponding X-ray energy dispersive spectroscopy (EDS) mapping results suggesting its fine nanostructure and uniform element distribution[4,28] (Figure S27, Supporting Information). CV curves were measured to test whether HT disturbed the reversible Zn^{2+}/H^{+} insertion/extraction behavior on the host structure. As shown in **Figure 5a**, ZFC displays multipeak, and increased response current with the scan rate and overlapped curves under the same rate, signifying highly reversible oxidation/reduction reactions.[29] Nevertheless, ZSO exhibits erratic curves with attenuated redox peak current under the same scans, corresponding to a continuous capacity fade process as the following lifespan test revealed (Figures S28,S29, Supporting Information). Self-discharge behavior under 60 °C was tracked, as Figure 5b suggested, ZFC held 73.77% capacity after 24 h, while only 51.82% in ZSO electrolyte (Figure 5c). The above results demonstrated that ZFC has depressed side reaction and energy dissipation reaction aggravated by HT during calendar aging time.[30] Additionally, the rate performance under various current densities from 0.2 to 2 A g^{-1} was tested in Figure 5d, it is self-evident that ZFC electrolyte compromised the rate performance at high current densities which on account of decreased ionic conductivity that dragged the ion transfer kinetics, especially under high current densities, thus incurring some extent rate capacity loss.[16] When current density switched back to 0.2 A g^{-1} after imposing various currents, outperformed capacity retention of ZFC than its counterpart revealed a ceaseless capacity fade in ZSO for the influence of highly active H_2O with NVO

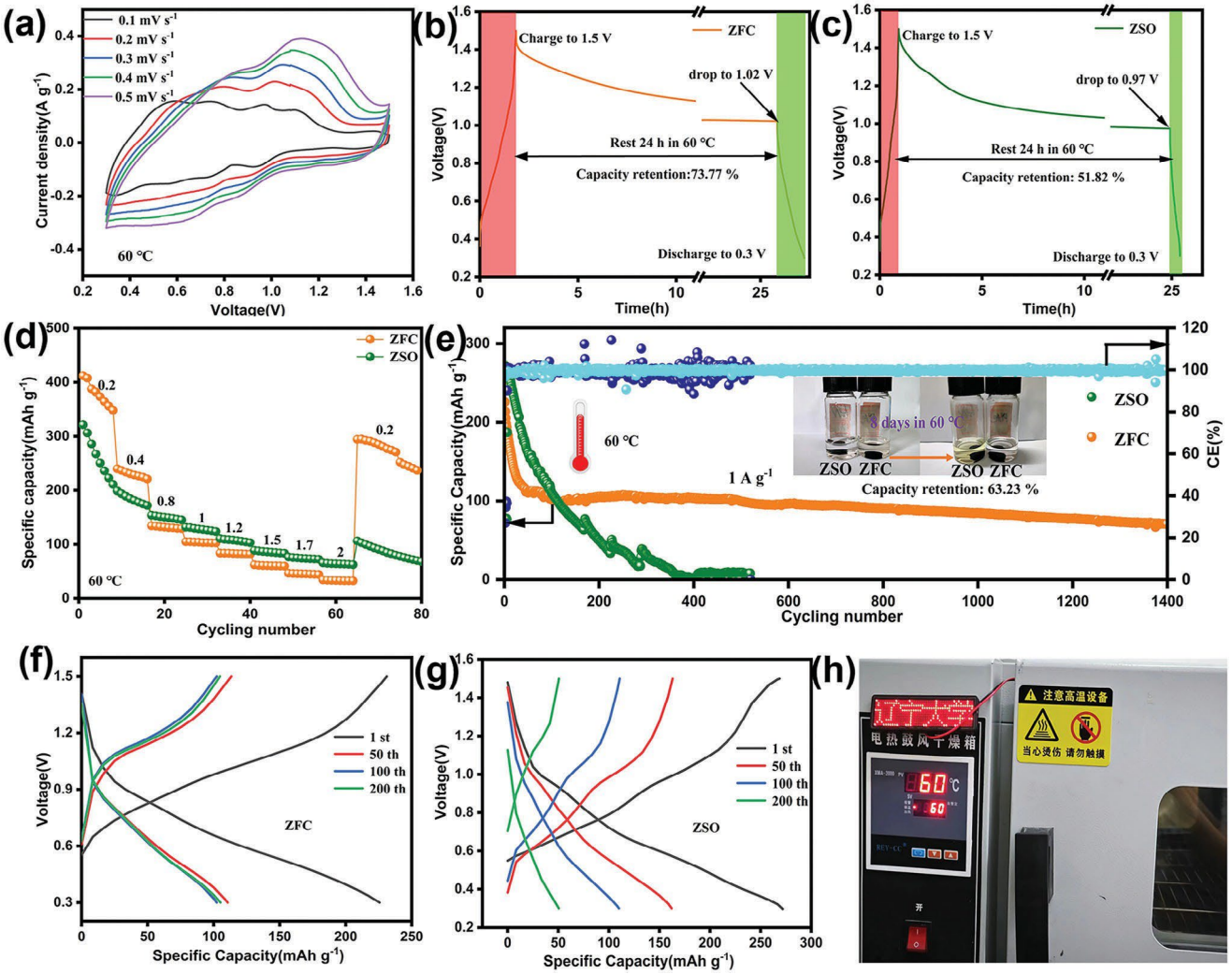

Figure 5. a) CV curves of ZFC electrolyte at 60 °C. Capacity retention test employing b) ZFC and c) ZSO electrolyte at 60 °C after 24 h rest. d) The rate performance of the above electrolyte. e) Long-term cycling performance of the above electrolyte. Inset: NVO cathode was exposed to ZFC and ZSO for 8 days at 60 °C. GCD profiles of f) ZFC and g) ZSO in 1st, 50th, 100th, 200th cycles. h) A Light sign was powered by Zn||NVO full cells with ZFC electrolyte at 60 °C.

host materials. The lifespan performance of two electrolytes was measured as well (Figure 5e), ZFC suffered a raid capacity fade at the beginning, which was attributed to a uniform SEI formation process, with the capacity of 111 mAh g^{-1} under 1A g^{-1} when in stable status, corresponding well with rate performance results, suggesting a depressed HT-triggered capacity fluctuation and sustained 1400 cycles with the capacity retention of 63.23%. Although initial ZSO capacity was superior to ZFC, its capacity shrunk to zero with unstable CE after 400 cycles. All of this suggested that ZFC compatibles well with NVO cathode at HT operation and hampers unregular deposition and side reactions to prevent capacity loss from happening.[16] Additionally, to visualize cathode stability at HT,[3] the NVO cathode was sealed into the above electrolytes, both electrolytes remained transparent and colorless before the soaking experiment. However, the ZSO electrolyte turned dark green while ZFC remained in its original state after 8 days. Ultraviolet-visible(UV–vis) spectra of the above electrolyte witnessed the high intensity of the absorption band from 300 to 500 cm^{-1} in ZSO due to electron transfer from O to V^{5+} for vanadium dissolution in Figure S30 (Supporting Information).[31] This phenomenon from ZFC electrolyte could attributed to host lattice integrity being maintained benefiting from reduced water activity for reconstructed hydrogen bond network and optimized solvation structure.[16,32] Their GCD profiles in Figure 5f,g in 1st, 50th, 100th, 200th cycles reaffirmed the advantages of ZFC over ZSO in long-term performance detailly. Furthermore, a powered light sign and mini fan with ZFC in the Zn||NVO full cells brought this electrolyte into a practical scenario (Figure 5h and Figure S31, Supporting Information), further unveiling the promising application potential at HT. Finally, the electrochemical performances of Zn||Zn symmetric cells and Zn||NVO full cells were tested at room temperature and 80 °C as Figure S32 showed, Figure S32a,c (Supporting Information) exhibited barely satisfactory performance for the

lifetime of Zn||Zn symmetric cells. Nevertheless, the results revealed that there is still a lot of potential for improvement in terms of capacity problems at room temperature as Figure S32b (Supporting Information) and stability at HT as Figure S32d (Supporting Information) displayed.

3. Conclusion

In summary, we introduced low-concentration zinc salt zinc trifluoroacetate, with TEP and H_2O to enable AZIBs to operate at HT, thus synergistic effect was realized. On the one hand, the original hydrogen bond network was reconstructed due to the intense interaction between TEP and H_2O. Consequently, the active water powered by HT was depressed, which was auspicious to frustrate the parasitic reaction and undesired corrosion. On the other hand, SEI was formed on zinc anode uniformly and tightly for the decomposition of introduced zinc salt. Meanwhile, uniform SEI separated the electrolyte and anode physically, preventing direct contact between active water and zinc anode, thus reducing the corrosion of active water. Moreover, TEP, rich in the polar functional group, was capable of preferentially anchored upon zinc anode as a shielding buffer layer. It was not only reshaping the structure of EDL but also assisting in the SEI formation promptly. As proof of this conception, the assembled Zn||Zn symmetrical cells sustained to 2000 h under the condition of 0.1 mA cm^{-2}, and the Zn||NVO full cells achieved 1400 cycles at 1 A g^{-1} with 63.23% capacity remaining at 60 °C. This work is expected to give a promising path to prompt the commercialization of AZIBs at HT.

Supporting Information

Supporting Information is available from the Wiley Online Library or from the author.

Acknowledgements

This work was supported by the National Natural Science Foundation of China (Nos. 52071171, 52202248), the Key Research Project of Department of Education of Liaoning Province (LJKZZ20220015), the Research Fund for the Doctoral Program of Liaoning Province (2022-BS-114), and theChunhui Program of the Ministry of Education of the People's Republic of China (202201135), the Liaoning University Youth Research Fund project (LDZDJB2302), Fundamental Research Funds for Public Universities in Liaoning (LJKLJ202425), the Natural Science Foundation of Liaoning Province (2024-MS-007), T.M. acknowledged the Australian Research Council (ARC) through Future Fellowship (FT210100298), the Discovery Project (DP220100603), the Linkage Project (LP210200504, LP220100088, LP230200897) and the Industrial Transformation Research Hub (IH240100009) schemes, the Australian Government through the Cooperative Research Centres Projects (CRCPXIII000077), the Australian Renewable Energy Agency (ARENA) as part of ARENA's Transformative Research Accelerating Commercialisation Program (TM021), and the European Commission's Australia-Spain Network for Innovation and Research Excellence (AuSpire). The authors also would like to thank Shiyanjia Lab (www.shiyanjia.com) for the XPS and SEM tests.

Conflict of Interest

The authors declare no conflict of interest.

Data Availability Statement

The data that support the findings of this study are available from the corresponding author upon reasonable request.

Keywords

high temperature zinc ion batteries, low concentration zinc salt, synergistic effect

Received: October 13, 2024
Revised: November 12, 2024
Published online: November 26, 2024

[1] a) F. Ye, R. Pang, C. Lu, Q. Liu, Y. Wu, R. Ma, L. Hu, *Angew. Chem., Int. Ed.* **2023**, *62*, 202303480; b) X. Zhang, Y. Liu, S. Wang, J. Wang, F. Cheng, Y. Tong, L. Wei, Z. Fang, J. Mao, *Energy Stor. Mater.* **2024**, *70*, 103471.

[2] J. Yang, B. Yin, Y. Sun, H. Pan, W. Sun, B. Jia, S. Zhang, T. Ma, *Nano-Micro Lett.* **2022**, *14*, 42.

[3] a) Y. Dai, C. Zhang, J. Li, X. Gao, P. Hu, C. Ye, H. He, J. Zhu, W. Zhang, R. Chen, W. Zong, F. Guo, I. P. Parkin, D. J. L. Brett, P. R. Shearing, L. Mai, G. He, *Adv. Mater.* **2024**, *36*, 2310645; b) D. Han, Z. Wang, H. Lu, H. Li, C. Cui, Z. Zhang, R. Sun, C. Geng, Q. Liang, X. Guo, Y. Mo, X. Zhi, F. Kang, Z. Weng, Q. H. Yang, *Adv. Energy Mater.* **2022**, *12*, 2102982; c) Y. Liu, C. Lu, Y. Yang, W. Chen, F. Ye, H. Dong, Y. Wu, R. Ma, L. Hu, *Adv. Mater.* **2024**, *36*, 2312982.

[4] a) Q. Zong, W. Du, C. Liu, H. Yang, Q. Zhang, Z. Zhou, M. Atif, M. Alsalhi, G. Cao, *Nano-Micro Lett.* **2021**, *13*, 116; b) H. Ren, S. Li, B. Wang, Y. Zhang, T. Wang, Q. Lv, X. Zhang, L. Wang, X. Han, F. Jin, C. Bao, P. Yan, N. Zhang, D. Wang, T. Cheng, H. Liu, S. Dou, *Adv. Mater.* **2023**, *35*, 2208237.

[5] a) J. Wang, J. X. Tian, G. X. Liu, Z. Z. Shen, R. Wen, *Small Methods* **2023**, *7*, 2300392; b) X. Bai, M. Sun, J. Yang, B. Deng, K. Yang, B. Huang, W. Hu, X. Pu, *Energy Environ. Sci.* **2024**, *17*, 7330; c) G. Qu, H. Wei, S. Zhao, Y. Yang, X. Zhang, G. Chen, Z. Liu, H. Li, C. Han, *Adv. Mater.* **2024**, *36*, 2400370.

[6] a) Z. Li, Y. Chen, X. Yun, P. Gao, C. Zheng, P. Xiao, *Adv. Funct. Mater.* **2023**, *33*, 2300502; b) Z. Xu, R. Ma, X. Wang, *Energy Storage Mater.* **2022**, *46*, 233.

[7] R. Wang, Q. Ma, L. Zhang, Z. Liu, J. Wan, J. Mao, H. Li, S. Zhang, J. Hao, L. Zhang, C. Zhang, *Adv. Energy Mater.* **2023**, *13*, 2302543.

[8] X. Yun, Y. Chen, H. Gao, D. Lu, L. Zuo, P. Gao, G. Zhou, C. Zheng, P. Xiao, *Adv. Energy Mater.* **2024**, *14*, 2304341.

[9] Z. Xing, G. Xu, J. Han, G. Chen, B. Lu, S. Liang, J. Zhou, *Trends Chem* **2023**, *5*, 380.

[10] a) J. Li, S. Qin, M. Xu, W. Wang, J. Zou, Y. Zhang, H. Dou, Z. Chen, *Adv. Funct. Mater.* **2024**, *34*, 2402186; b) N. Yahaya, A. H. Mohamed, M. Sajid, N. N. M. Zain, P. C. Liao, K. W. Chew, *Carbohydr. Polym.* **2024**, *338*, 122199.

[11] K. Guan, W. Chen, Y. Yang, F. Ye, Y. Hong, J. Zhang, Q. Gu, Y. Wu, L. Hu, *Adv. Mater.* **2024**, *36*, 2405889.

[12] L. Wang, C. Shen, C. Huang, J. Chen, J. Zheng, *ACS Nano* **2023**, *17*, 24619.

[13] W. Wang, S. Chen, X. Liao, R. Huang, F. Wang, J. Chen, Y. Wang, F. Wang, H. Wang, *Nat. Commun.* **2023**, *624*, 14.

[14] a) D. Wang, D. Lv, H. Peng, C. Wang, H. Liu, J. Yang, Y. Qian, *Angew. Chem., Int. Ed.* **2023**, *62*, 202310290; b) W. Song, X. Xie, L. Deng, A. Pan, G. Cao, S. Liang, G. Fang, *Energy Storage Mater.* **2024**, *70*, 103489.

[15] a) J. Zhu, M. Yang, Y. Hu, M. Yao, J. Chen, Z. Niu, *Adv. Mater.* **2023**, *36*, 2304426; b) X. Luo, M. Zhou, Z. Luo, T. Shi, L. Li, X. Xie,

Y. Sun, X. Cao, M. Long, S. Liang, G. Fang, *Energy Storage Mater.* **2023**, *57*, 628; c) C. Liao, L. Han, W. Wang, W. Li, X. Mu, Y. Kan, J. Zhu, Z. Gui, X. He, L. Song, Y. Hu, *Adv. Funct. Mater.* **2023**, *33*, 2212605.

[16] a) Z. Hu, Z. Song, Z. Huang, S. Tao, B. Song, Z. Cao, X. Hu, J. Wu, F. Li, W. Deng, H. Hou, X. Ji, G. Zou, *Angew. Chem., Int. Ed.* **2023**, *62*, 202309601; b) Z. Chen, Y. Wang, Q. Wu, C. Wang, Q. He, T. Hu, X. Han, J. Chen, Y. Zhang, J. Chen, L. Yang, X. Wang, Y. Ma, J. Zhao, *Adv. Mater.* **2024**, *36*, 2411004.

[17] W. Xu, J. Li, X. Liao, L. Zhang, X. Zhang, C. Liu, K. Amine, K. Zhao, J. Lu, *J. Am. Chem. Soc.* **2023**, *145*, 22456.

[18] R. Chen, W. Zhang, C. Guan, Y. Zhou, I. Gilmore, H. Tang, Z. Zhang, H. Dong, Y. Dai, Z. Du, X. Gao, W. Zong, Y. Xu, P. Jiang, J. Liu, F. Zhao, J. Li, X. Wang, G. He, *Angew. Chem., Int. Ed.* **2024**, *63*, 202401987.

[19] Y. Meng, M. Wang, J. Wang, X. Huang, X. Zhou, M. Sajid, Z. Xie, R. Luo, Z. Zhu, Z. Zhang, N. A. Khan, Y. Wang, Z. Li, W. Chen, *Nat. Commun.* **2024**, *15*, 8431.

[20] X. Zhao, Y. Wang, C. Huang, Y. Gao, M. Huang, Y. Ding, X. Wang, Z. Si, D. Zhou, F. Kang, *Angew. Chem., Int. Ed.* **2023**, *135*, 202312193.

[21] Y. Lyu, J. A. Yuwono, P. Wang, Y. Wang, F. Yang, S. Liu, S. Zhang, B. Wang, K. Davey, J. Mao, Z. Guo, *Angew. Chem., Int. Ed.* **2023**, *62*, 202303011.

[22] X. Shi, J. Xie, J. Wang, S. Xie, Z. Yang, X. Lu, *Nat. Commun.* **2024**, *15*, 302.

[23] F. Liu, Y. Zhang, G. Li, J. Jiang, L. Chen, T. Song, Y. Pei, X. Wang, X. Wu, B. Long, *Chem. Eng. J.* **2024**, *493*, 152526.

[24] T. Long, Q. Y. Zhao, G. Y. Yin, P. X. Xie, S. L. Liu, X. Ma, Q. Wu, B. Y. Lu, Z. H. Dai, X. X. Zeng, *Adv. Funct. Mater.* **2024**, *34*, 2315539.

[25] Y. Deng, Y. Wu, K. Zhang, M. Fan, L. Wang, Y. He, L. Yan, *J. Mater. Chem. A* **2023**, *11*, 8368.

[26] C. Meng, W.-D. He, H. Tan, X.-L. Wu, H. Liu, J.-J. Wang, *Energy Environ. Sci.* **2023**, *16*, 3587.

[27] Y. Zhao, T. Zhou, L. P. H. Jeurgens, X. Kong, J. W. Choi, A. Coskun, *Chem* **2023**, *9*, 682.

[28] Q. Li, X. Rui, D. Chen, Y. Feng, N. Xiao, L. Gan, Q. Zhang, Y. Yu, S. Huang, *Nano-Micro Lett.* **2020**, *12*, 67.

[29] Z. Wu, C. Lu, F. Ye, L. Zhang, L. Jiang, Q. Liu, H. Dong, Z. Sun, L. Hu, *Adv. Funct. Mater.* **2021**, *31*, 2106816.

[30] Z. Wu, F. Ye, Q. Liu, R. Pang, Y. Liu, L. Jiang, Z. Tang, L. Hu, *Adv. Energy Mater.* **2022**, *12*, 2270097.

[31] Z. Tao, J. Cui, Y. Tan, Z. Zhou, Z. Chen, A. Wang, Y. Zhu, S. Lai, M. Yu, Y. Yang, *Small* **2023**, *19*, 2301620.

[32] a) S. Liu, J. He, D.-s. Liu, M. Ye, Y. Zhang, Y. Qin, C. C. Li, *Energy Stor. Mater.* **2022**, *49*, 93; b) Y. Zhong, X. Xie, Z. Zeng, B. Lu, G. Chen, J. Zhou, *Angew. Chem., Int. Ed.* **2023**, *62*, 202310577.